



A comparative study of wet etching and contacts on $(\bar{2}01)$ and (010) oriented $\beta\text{-Ga}_2\text{O}_3$

Soohwan Jang ^a, Sunwoo Jung ^a, Kimberly Beers ^b, Jiancheng Yang ^c, Fan Ren ^c, A. Kuramata ^d, S.J. Pearton ^b, Kwang Hyeon Baik ^{e,*}

^a Department of Chemical Engineering, Dankook University, Yongin, 16890, Republic of Korea

^b Department of Materials Science and Engineering, University of Florida, Gainesville, FL, 32611, USA

^c Department of Chemical Engineering, University of Florida, Gainesville, FL, 32611, USA

^d Tamura Corporation and Novel Crystal Technology, Inc., Sayama-shi, Saitama, 350-1328, Japan

^e School of Materials Science and Engineering, Hongik University, Jochiwon, Sejong, 30016, Republic of Korea

ARTICLE INFO

Article history:

Received 27 July 2017

Accepted 30 September 2017

Available online 3 October 2017

Keywords:

Ga_2O_3
Wet etching
Ohmic contact
Monoclinic
Dangling bond

ABSTRACT

We report on the effect of $\beta\text{-Ga}_2\text{O}_3$ crystal orientation on wet etching and Ohmic contact formation. The photochemical etching rate in KOH solutions of $(\bar{2}01)$ oriented, n-type bulk single crystals grown by the edge-defined film-fed growth method is ~3–4 times higher than for the (010) planes. The activation energy for etching was 0.498 eV and 0.424 eV for (201) and (010) orientations, respectively, suggesting the etching is reaction-limited with the same rate-limiting step. Ti (200 Å)/Au (1500 Å) metallization deposited on the two different orientations and annealed at 450 °C showed Ohmic current-voltage (*I-V*) behavior for $(\bar{2}01)$ but rectifying characteristics for (010) . For $(010)\text{ Ga}_2\text{O}_3$, there exists 2 types of surfaces having Ga and O atomic densities of 0.58 and $0.87 \times 10^{15} \text{ cm}^{-2}$, respectively. By contrast, for $(\bar{2}01)\text{ Ga}_2\text{O}_3$ surfaces, there exist 2 types of surface, with each type terminated with only Ga or O. If the surface is terminated with O, the dangling bond densities of O are 1.78 and $2.68 \times 10^{15} \text{ cm}^{-2}$, respectively. We found that $(\bar{2}01)$ -oriented Ga_2O_3 is etched at higher rates and is easier to form Ohmic contacts than $(010)\text{ Ga}_2\text{O}_3$. The higher density of oxygen dangling bonds on the $(\bar{2}01)$ plane correlates with the faster etch rates and pronounced Ohmic behavior from deposited metals.

© 2017 Elsevier B.V. All rights reserved.

1. Introduction

The $\beta\text{-Ga}_2\text{O}_3$ polymorph is a monoclinic structure that is attracting interest for power electronic devices, as well as solar-blind UV photodetectors, gas sensors and transparent conducting films for electrodes on a variety of optoelectronic devices [1–15]. There are a number of other polymorphs of Ga_2O_3 , including the corundum (α), defective spinel (γ), hexagonal (ε) and the orthorhombic (κ), but recent attention has focused on the monoclinic $\beta\text{-Ga}_2\text{O}_3$ structure [1,2]. There are a number of orientations of $\beta\text{-Ga}_2\text{O}_3$ in common use, including the $(\bar{2}01)$, (010) and (001) planes [4,6,9,11]. In material grown by the edge-defined film-fed growth method [4], the (010) oriented crystals can be cut to produce $(\bar{2}01)$ planes in the specific crystallographic direction.

There is obviously interest in the difference of physical, optical

and electrical properties of these crystal orientations due to the crystalline anisotropy. For example, the thermal conductivity in Ga_2O_3 shows a strong anisotropy, with the $[010]$ direction showing a thermal conductivity 2.5 times higher than that in the $[100]$ direction [2,16–19], although both theory and experiment suggest there is little anisotropy in electron effective mass [2]. The $(\bar{2}01)$ and (010) surfaces differ significantly in terms of their dangling bond densities of oxygen, and this might be expected to have an effect on processes like wet etching or metal contact formation. Wet etching is needed for patterning features on the Ga_2O_3 for device fabrication, while high quality Ohmic and rectifying contacts are needed for diode rectifiers and transistors. It has already been reported that the wet etching rate of (100) oriented Ga_2O_3 was almost double that of (001) crystals in 47% HF solutions at 25 °C [20]. H_3PO_4 was found to etch $\beta\text{-Ga}_2\text{O}_3$ (100) substrates at rates up to several hundred nm/min at temperatures < 200 °C [21]. H_3PO_4 wet etching at 130 °C for several hours has been used to estimate dislocation densities in $(\bar{2}01)$ and $(010)\text{ Ga}_2\text{O}_3$ by counting etch pits [4]. These were either triangular or line shaped and were found to

* Corresponding author.

E-mail address: kbaik@hongik.ac.kr (K.H. Baik).

correlate with dislocation density using transmission electron microscopy. Other wet etchants have been reported for Ga_2O_3 include HNO_3/HCl , H_2SO_4 , and HF-based solutions [20–23]. For dry etching of $\beta\text{-Ga}_2\text{O}_3$, Hogan et al. reported a maximum etch rate of 43 nm/min with BCl_3 using the inductively coupled plasma etching technique. The authors found similar etch rates for (010) and ($\bar{2}01$) planes, and slower etch rates for the (100) due to the surface oxygen anions and lower density of dangling bonds [24]. Yao et al. also reported recently that surface states appear to have a more dominant effect on Schottky diode characteristics than the actual choice of metal [25]. Thus, the orientation of the wafer surface, which defines both the Ga-to-O ratio and the density of dangling bond states, is a major consideration when examining surface-controlled processes. In this paper, we show that the photo-enhanced chemical (PEC) etch rates of Ga_2O_3 are much faster on ($\bar{2}01$) planes than on (010) and it is much easier to form Ohmic contacts on the former.

2. Experimental

The starting samples were bulk β -phase Ga_2O_3 single crystal wafers with (201) and (010) surface orientations (Tamura Corporation, Japan) grown by the edge-defined film-fed growth method [4]. Hall Effect measurements showed these Sn-doped samples were both n-type with an electron concentration of $\sim 10^{18} \text{ cm}^{-3}$. This is an important fact for the experiments in which we compare contact properties for metals deposited on the two different orientations. The front side of the samples was chemically mechanically polished after cutting from the original bulk crystal. The dislocation density determined by etch pit measurements was around 10^3 cm^{-2} [4]. The crystal quality was examined by X-Ray Diffraction (XRD) and photoluminescence (PL) measurements. The excitation source in the latter case was a 266 nm Nd:YAG laser with a filter (<290 nm) to cut off the laser reflection into the detector. XRD studies were performed on a Philips PW3040 diffractometer

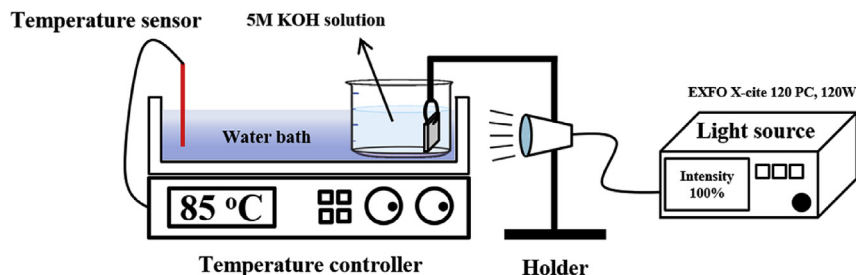


Fig. 1. Schematic of PEC etch system.

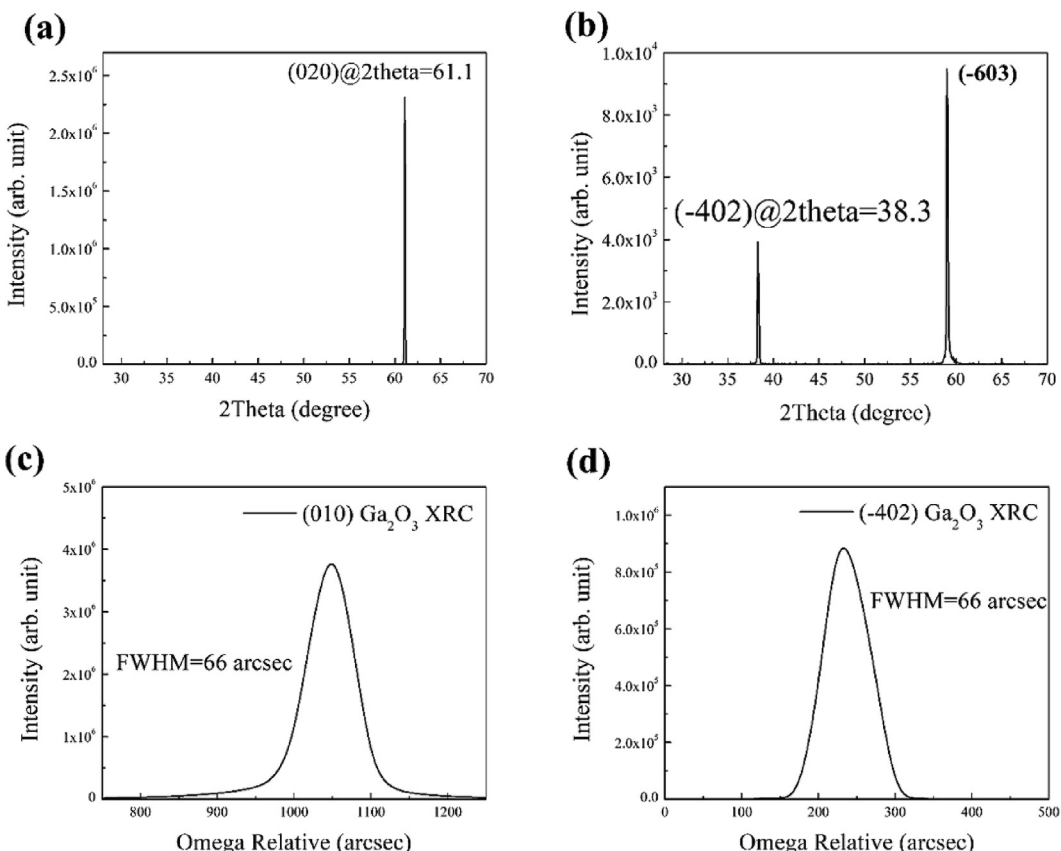


Fig. 2. θ - 2θ diffraction patterns (top) and x-ray rocking curves from the (020) and ($\bar{4}02$) diffraction peaks, respectively, (bottom) from the (010) (left) and ($\bar{2}01$) (right) wafers.

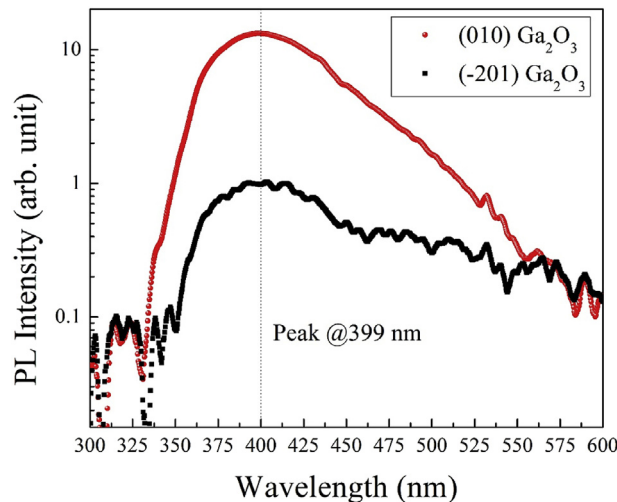


Fig. 3. PL spectra from (010) and ($\bar{2}01$) Ga_2O_3 wafers.

with a PW3020 goniometer equipped with the thin film package including a graphite monochromator. Cu $\text{K}\alpha_1$ X-ray target source ($\lambda = 1.5406 \text{ \AA}$) was used, while the instrumental resolution in θ - 2θ

modes was about $0.1''$ in 2θ and in the X-ray rocking curve modes about $0.15''$ in ω .

For PEC etching, both ($\bar{2}01$) and (010) Ga_2O_3 single crystal wafers were immersed in a 5 M potassium hydroxide (KOH) solution for 30 min at a stirring rate of 300 rpm at $80\text{--}95^\circ\text{C}$ with ultraviolet illumination from a 120 W Hg lamp [26,27]. The emission bands from the lamp range from above bandgap all the way to the yellow-orange region (578.2 nm). A schematic of the system is shown in Fig. 1. The etched surface morphologies of the ($\bar{2}01$) and (010) wafers were analyzed by a field emission scanning electron microscope (SEM). The contact properties of Ti (200 \AA)/Au (1500 \AA) bilayer metal stacks deposited by liftoff and annealed at 450°C for 1 min under a flowing N_2 ambient were examined by current-voltage (I-V) measurements at 25°C . No reactive ion etching was performed to enhance the conductivity of the surface prior to the metallization.

3. Results and discussion

3.1. Materials characterization

Fig. 2(a) and (b) show the XRD results for the two types of samples, with typical θ - 2θ diffraction patterns of (010) and ($\bar{2}01$) oriented $\beta\text{-Ga}_2\text{O}_3$. The only reflections obtained are (020) for the

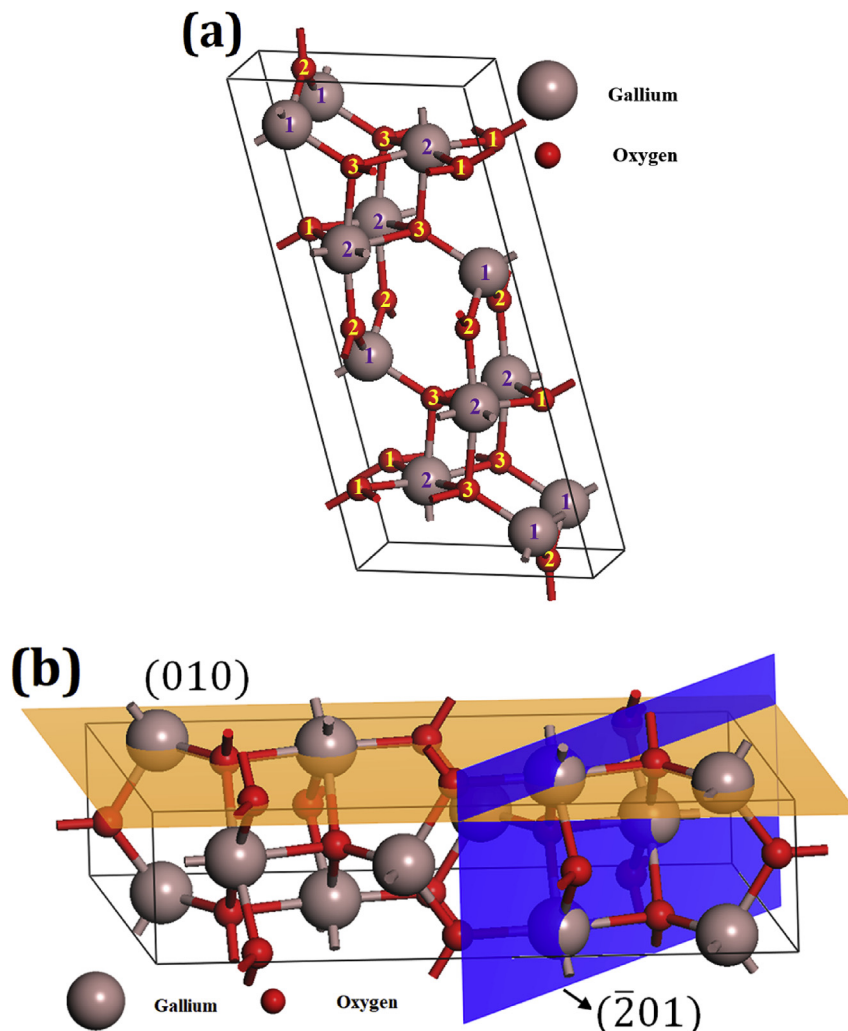


Fig. 4. (a) $\beta\text{-Ga}_2\text{O}_3$ crystal structure and (b) (010) and ($\bar{2}01$) surfaces.

(010) sample and (−402) and (−603) for the (−201) orientations. Both samples display the full-width at half-maximum (FWHM) of 66 arcsecs from the rocking curves shown in Fig. 2(c) and (d), consistent with their low dislocation density and excellent crystal quality.

Fig. 3 shows the room temperature PL spectra from the two types of samples. The spectra are dominated by a broad set of transitions centered near 399 nm which have previously been ascribed to oxygen-vacancy related transitions. Dong et al. [28] reported four bands in this region, with the one at 380 nm in the UV region suggested to be caused by transition levels between the oxygen vacancy and unintended N impurities. They also reported peaks centered at 416 nm, 442 nm (both in the violet region) and 464 nm (blue region), with all three emission peaks suggested to originate from the electron-hole recombination formed by oxygen vacancies, or to the recombination of Ga-O vacancy pair [28–33]. The formation energy of the oxygen vacancies of β -Ga₂O₃ has been investigated in the past years, and the results can vary with different functional and approximation methods [1,2,34,35]. Historically, Ga₂O₃ has shown three different groups of emission bands, in the UV (3.2–3.6 eV), blue (2.8–3.0 eV), and green (2.4 eV) regions [36–39], but it is fair to suggest that the specific origins of the transitions are not finalized.

3.2. Crystal structure and surface atom density differences

The characteristics of wet etching and metal contact on (−201) and (010) Ga₂O₃ surfaces are expected to be significantly different depending on the crystal orientations in terms of atomic arrangements, surface energy and their dangling bond densities of both Ga and O atoms. Thus, it is necessary to examine the difference in atomic configurations in detail for both (−201) and (010) Ga₂O₃ crystal surfaces.

Fig. 4(a) shows the monoclinic crystal structure of Ga₂O₃ with

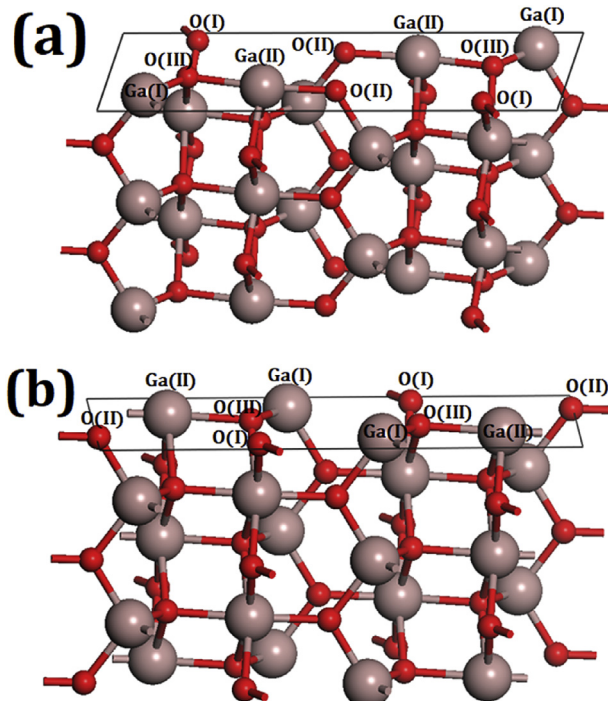


Fig. 5. Atomic bond configurations of (a) type I Ga₂O₃ (010) surfaces. Brown and red spheres represent Ga and O atoms, respectively. (For interpretation of the references to colour in this figure legend, the reader is referred to the web version of this article.)

lattice parameters of $a = 12.23 \text{ \AA}$, $b = 3.04 \text{ \AA}$, $c = 5.8 \text{ \AA}$, and $\theta = 103.7^\circ$, in which there exist two inequivalent Ga sites and three inequivalent O sites, denoted by Ga(I), Ga(II), O(I), O(II), and O(III) atoms, respectively. Ga(I) atoms form slightly distorted tetrahedral bonds with 4 O ions, and Ga(II) atoms form a highly distorted cubic close packing arrangement with 6 neighboring O ions. O(I) and O(II) are 3-fold-coordinated, whereas O(III) is 4-fold-coordinated at the corner of three octahedra and one tetrahedron [40–42]. Fig. 4(b) shows schematics of the (010) plane (brown) and (−201) plane (blue). It is clear that the atomic arrangement for each crystal plane is different, thus leading to different atomic configuration and dangling bond density on a particular crystal orientation. The (010) plane consist of Ga (I) atoms in tetrahedral site and Ga (II) in octahedral site, and O atoms in a distorted octahedral arrangement. It is notable that respective Ga and O atoms have different numbers of dangling bonds depending on the sites of the Ga₂O₃ surface, as

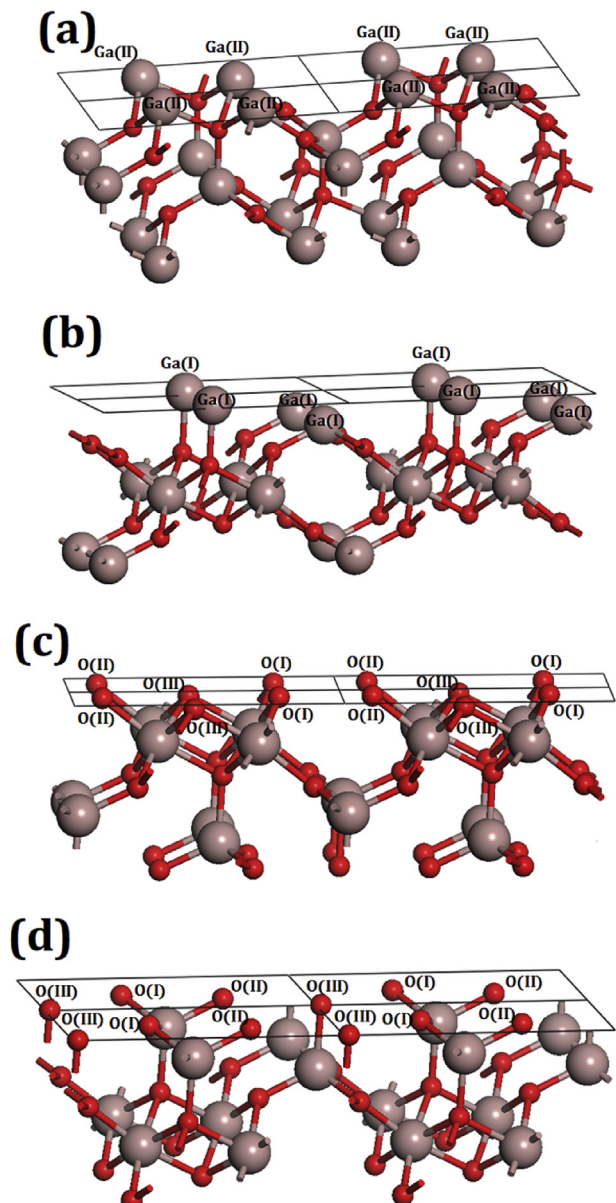


Fig. 6. (a) Ga-terminated (−201) surfaces (type I), (b) Ga-terminated (−201) surfaces (type II), (c) O-terminated (−201) surfaces (type I), and (d) O-terminated (−201) surfaces (type II).

Table 1

Summary of atomic and dangling bond densities on the faces of the various orientations examined. The results were obtained from simulations.

Crystal structure	Ga atoms ($\times 10^{15} \text{ cm}^{-2}$)	O atoms ($\times 10^{15} \text{ cm}^{-2}$)	Gallium dangling bond ($\times 10^{15} \text{ cm}^{-2}$)	Oxygen dangling bond ($\times 10^{15} \text{ cm}^{-2}$)
(010) Type I	0.58	0.87	0.87	0.87
(010) Type II	0.58	0.87	0.87	0.87
($\bar{2}01$) Ga-terminated type I	0.89	0	2.68	0
($\bar{2}01$) O-terminated type I	0	1.34	0	1.78
($\bar{2}01$) Ga-terminated type II	0.89	0	1.78	0
($\bar{2}01$) O-terminated type II	0	1.34	0	2.68

follows; 4-fold-coordinated Ga(I) with the number of dangling bonds of 1 and 3, 6-fold-coordinated Ga(II) with 2 and 3 dangling bonds, 3-fold-coordinated O(I) with 1 dangling bond, 3-fold-coordinated O(II) with 1 and 2 dangling bonds, 4-fold-coordinated O(III) with 1 and 3 dangling bonds. The atomic densities can be calculated for which the parameters were determined from plots of the crystal structure, an example of which is shown in Fig. 4. The number of dangling bonds for Ga or O can be then calculated in a similar fashion, using the number of bonds formed to each atom and the

number of atoms per unit cell.

For (010) Ga_2O_3 as shown in Fig. 5(a) and (b), there exists 2 types of surfaces with Ga atomic density of $0.58 \times 10^{15} \text{ cm}^{-2}$ and O of $0.87 \times 10^{15} \text{ cm}^{-2}$. The dangling bond densities of Ga and O atoms on for both (010) surfaces are estimated to be the same, $0.58 \times 10^{15} \text{ cm}^{-2}$ and $0.87 \times 10^{15} \text{ cm}^{-2}$ for Ga and O atoms, respectively. Fig. 6(a)–(d) shows the possible ($\bar{2}01$) Ga_2O_3 surfaces, 2 types of surface, in which each type is terminated with only Ga or O. For the two types of ($\bar{2}01$) surfaces, the Ga and O atomic densities are $0.89 \times 10^{15} \text{ cm}^{-2}$ and $1.34 \times 10^{15} \text{ cm}^{-2}$, respectively. If the surface is terminated with O, the dangling bond densities of O are 1.78 and $2.68 \times 10^{15} \text{ cm}^{-2}$, respectively, for type I and II. Table 1 summarizes the results of these calculations, clearly indicating that the O dangling bond density for ($\bar{2}01$) surface is 2–3 times higher than for (010) surface.

3.3. PEC etching and surface morphology

PEC etching is an effective technique for anisotropic and

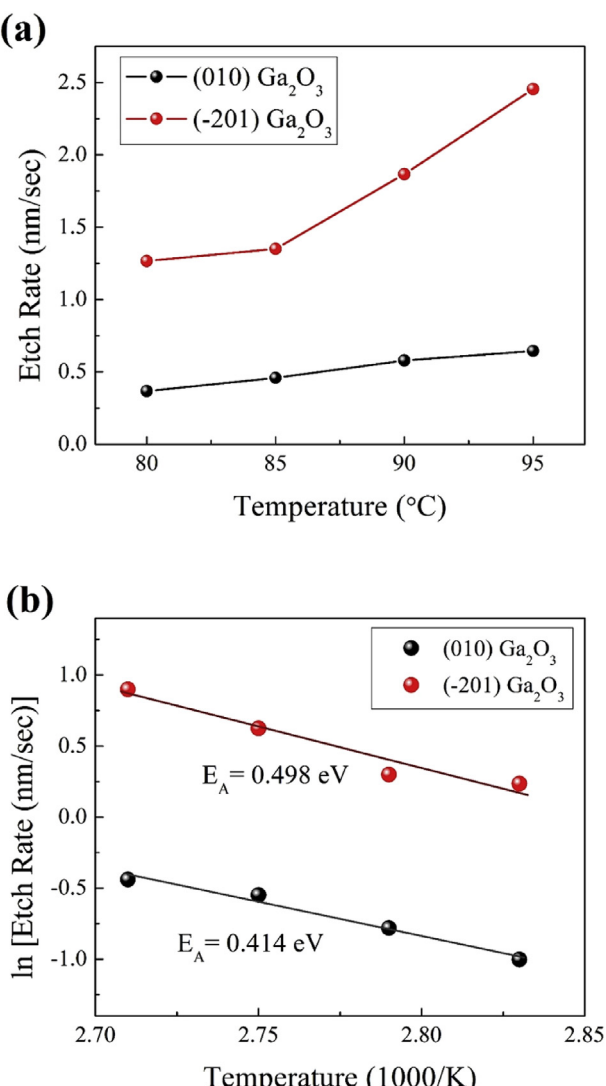


Fig. 7. (a) PEC etch rate versus solution temperature for ($\bar{2}01$) and (010) Ga_2O_3 wafers. The etch rates for ($\bar{2}01$)-oriented Ga_2O_3 are approximately 4 times higher for and (010)-oriented Ga_2O_3 . (b) Arrhenius plot of PEC etch rate for ($\bar{2}01$) and (010) Ga_2O_3 wafers.

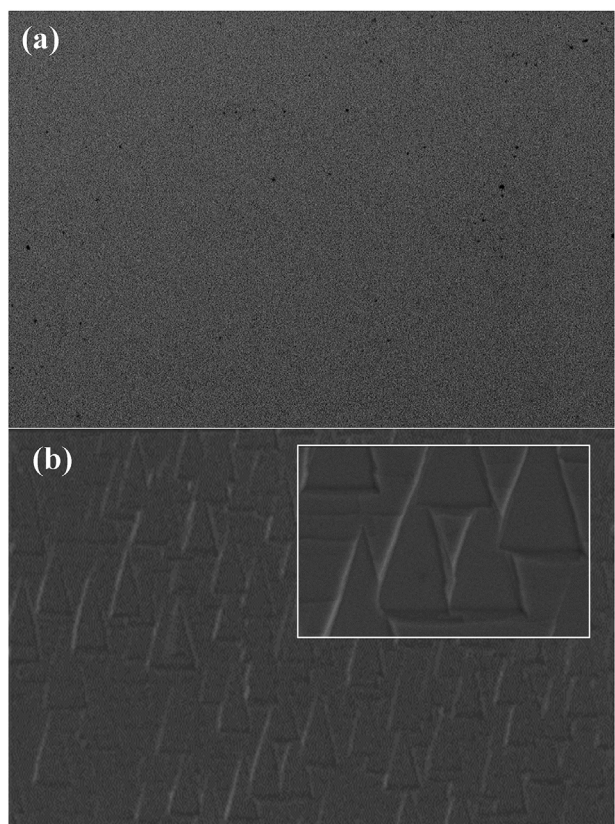


Fig. 8. SEM images of the surface morphology of (a) (010) and (b) ($\bar{2}01$) after PEC etching for 120 min at 95 °C. All the scale bars indicate 10 μm . The inset is the magnified SEM image.

bandgap-selective etching in wide bandgap semiconductors. We found it was also effective with β -Ga₂O₃. Note that both the $(\bar{2}01)$ and (010) surfaces remained intact in the etchant solution without UV illumination. Fig. 7(a) shows the PEC etch rates as a function of temperature for the two different orientations. The removal rates for the $(\bar{2}01)$ orientation was approximately three to four times faster than for the (010) . Note that the average etch depths were in the range 10–74 nm, depending on orientation and temperature for the 30 min etch times. The activation energy for etching was determined from Arrhenius plots, as shown in Fig. 7(b). For both orientations, the activation energy for the $(\bar{2}01)$ Ga₂O₃ crystals was 0.498 eV, which was slightly higher than the one for the (010) (0.414 eV). This energy is characteristic of that expected for reaction-limited etching, whose other characteristics include a linear increase in etch depth with time and an independence of etch rate on solution agitation [40]. SEM images of the surface morphology of the two types of samples after being etched for 120 min at 95 °C are shown in Fig. 8. It is quite interesting to see that triangular shape was formed on the surface of the $(\bar{2}01)$ Ga₂O₃ after KOH PEC etching. By contrast, the (010) surfaces maintained flat and smooth after the etching of approximately 10–19 nm depth.

As shown in Fig. 9(a), each side of the isosceles triangle with an angle of 70° was found to be (115) and $(\bar{1}\bar{1}5)$ planes, and the base is (010) plane. Fig. 9(b) shows the atomic bond configurations of the cleaved (115) and $(\bar{1}\bar{1}5)$ planes, demonstrating that Ga and O atoms coexist on those planes. In the case of Ga-O coexisting surface, OH[−] ions may form Ga-O compounds with Ga dangling bonds, but these are not easily soluble due to strong Ga-O bonding in the plane and the repulsive force between Ga-O bonds and OH[−] ions. Consequently, wet etching may be impeded on (115) , $(\bar{1}\bar{1}5)$ and (010) planes in Ga₂O₃, thus resulting in chemically stable surfaces in KOH wet chemicals under UV illumination.

The number of dangling bonds on the surface is believed to control the etching behavior of the different orientations of Ga₂O₃. For example, on an oxygen-terminated surface, the oxygen atoms which exists on the surface after removing the first Ga-layer by OH[−] ions, have dangling bonds. In KOH-based wet etching, it was suggested that Ga atoms react with OH[−] to also form Ga₂O₃, which subsequently dissolved in base solutions. In H₃PO₄-based etching, the Ga₂O₃ was suggested to dissolve directly in the acid solution. Clearly, in the case of Ga₂O₃, we can expect that the difference in Ga-to-O ratio and the dangling bond density on different planes will play a strong role in the PEC etching behavior. The $(\bar{2}01)$ -oriented Ga₂O₃ crystal etches roughly three to four times faster under PEC conditions in KOH solutions. We speculate that the higher etch rates for the $(\bar{2}01)$ Ga₂O₃ may be due to the higher density of O dangling bonds, which are exposed on the surface. As shown in Table 1, the O dangling bond density for $(\bar{2}01)$ surface is 2–3 times higher than for (010) surface. Thus, it can be said that (010) surface is more chemically stable than the $(\bar{2}01)$ surface due to low surface energy.

3.4. Contact property differences

Fig. 10 shows I-V characteristics at 25 °C of Ti/Au contacts deposited on either $(\bar{2}01)$ or (010) Sn-doped Ga₂O₃ wafers and then annealed at 450 °C for 5 min. Note that the contacts on the $(\bar{2}01)$ wafer shows Ohmic behavior, while in sharp contrast, those on the (010) wafer show rectifying behavior. Since the net doping density in both samples is the same, this indicates that the surface chemistry determines the effective barrier height and hence the dominant carrier transport mechanism. Interface-induced gap states, made up of both valence-band and conduction-band states in electronic oxides, often play a determining role in the barrier

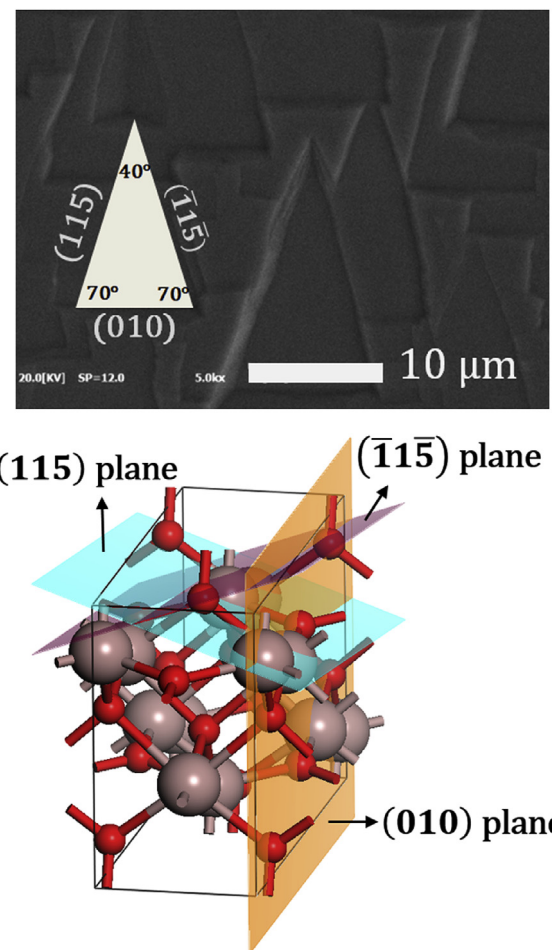


Fig. 9. (a) SEM image of the etched surface with Miller plane indices, (b) the crystal structure of (115) , $(\bar{1}\bar{1}5)$ and (010) planes of Ga₂O₃.

heights of metal contacts and some have noted a correlation between Schottky barrier heights for metals on Ga₂O₃ and the electronegativity difference between it and the metal [43]. Several

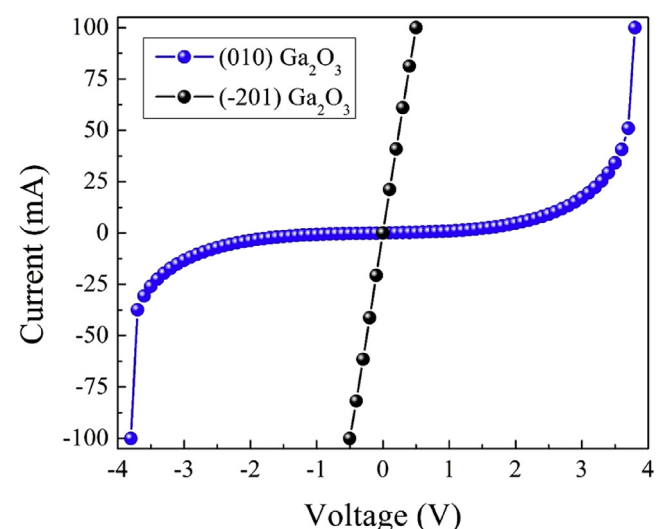


Fig. 10. I-V characteristics at 25 °C of Ti/Au contacts deposited on either $(\bar{2}01)$ or (010) Sn-doped Ga₂O₃ wafers and then annealed at 450 °C for 5 min.

authors have found that the presence of upward band bending in low conductivity Ga_2O_3 complicates achievement of Ohmic contacts [44–49], and there was a strong dependence of the properties of the barrier height on the energy of incident atoms during deposition. The latter implicates surface defects and stoichiometry as being key to determining the contact nature. The higher density of oxygen dangling bonds on the $(\bar{2}01)$ plane we are using here correlates with the faster etch rates and pronounced Ohmic behavior from deposited metals. This is not surprising since as discussed earlier, both the wet etch rate and effective barrier height depend on the surface chemistry and reactive bond density.

4. Summary and conclusions

The $(\bar{2}01)$ and (010) orientations of $\beta\text{-}\text{Ga}_2\text{O}_3$ doped at the same n-type conductivity and with similar structural quality exhibit different wet etching and contact properties. The $(\bar{2}01)$ orientation etches roughly three to four times faster under PEC conditions in KOH solutions, while also producing Ohmic contact behavior for Ti/Au contacts annealed at 450°C . This behavior is correlated with the oxygen dangling bond density on the respective surfaces and may provide a clue as to reported variations in barrier heights for common metals on $\beta\text{-}\text{Ga}_2\text{O}_3$. In such oxide systems, surface disorder, oxide surface polarity and role of atmospheric exposure prior to metal deposition and interfacial disorder after deposition may all influence the resulting contact properties. It is also likely that the different polymorphs of Ga_2O_3 will have different etching and contact properties for the same reasons.

Acknowledgments

This research was supported by the Basic Science Research Program through the National Research Foundation of Korea (NRF) funded by the Ministry of Education (2015R1D1A1A01058663, 2017R1D1A3B03035420), and Nano Material Technology Development Program through the National Research Foundation of Korea (NRF) funded by the Ministry of Science, ICT and Future Planning (2015M3A7B7045185). The project or effort depicted was also sponsored by the Department of Defense, Defense Threat Reduction Agency, HDTRA1-17-1-011, monitored by Jacob Calkins. The content of the information does not necessarily reflect the position or the policy of the federal government, and no official endorsement should be inferred. Part of the work at Tamura was supported by “The research and development project for innovation technique of energy conservation” of the New Energy and Industrial Technology Development Organization (NEDO), Japan. We also thank Dr. Kohei Sasaki from Tamura Corporation for fruitful discussions.

References

- [1] H. von Wenckstern, Group-III sesquioxides: growth, physical properties and devices, *Adv. Electron. Mater.* 3 (2017), 1600350.
- [2] S.I. Stepanov, V.I. Nikolaev, V.E. Bougov, A.E. Romanov, Gallium oxide: properties and applications - a review, *Rev. Adv. Mater. Sci.* 44 (2016) 63–86.
- [3] M.J. Tadjer, N.A. Mahadih, V.D. Wheeler, E.R. Glaser, L. Ruppalt, A.D. Koehler, K.D. Hobart, C.R. Eddy Jr., F.J. Kub, Communication—a (001) $\beta\text{-}\text{Ga}_2\text{O}_3$ MOSFET with $+2.9$ V threshold voltage and HfO_2 gate dielectric, *ECS J. Solid State Sci. Technol* 5 (2016) P468–P470.
- [4] A. Kuramata, K. Koshi, S. Watanabe, Y. Yamaoka, T. Masui, S. Yamakoshi, High-quality $\beta\text{-}\text{Ga}_2\text{O}_3$ single crystals grown by edge-defined film-fed growth, *Jpn. J. Appl. Phys.* 55 (2016), 1202A2.
- [5] M.A. Mastro, A. Kuramata, J. Calkins, J. Kim, F. Ren, S.J. Pearton, Opportunities and future directions for Ga_2O_3 , *ECS J. Solid State Sci. Technol* 6 (2017) P356–P359.
- [6] O. Ueda, N. Ikenaga, K. Koshi, K. Iizuka, A. Kuramata, K. Hanada, T. Moribayashi, S. Yamakoshi, M. Kasu, Structural evaluation of defects in $\beta\text{-}\text{Ga}_2\text{O}_3$ single crystals grown by edge-defined film-fed growth process, *Jpn. J. Appl. Phys.* 55 (2016), 1202BD.
- [7] N.A. Moser, J.P. McCandless, A. Crespo, K.D. Leedy, A.J. Green, E.R. Heller, K.D. Chabak, N. Peixoto, G.H. Jessen, High Pulsed Current Density $\beta\text{-}\text{Ga}_2\text{O}_3$ MOSFETs Verified by an Analytical Model Corrected for Interface Charge, vol. 110, 2017, 143505.
- [8] K. Zeng, J.S. Wallace, C. Heimburger, K. Sasaki, A. Kuramata, T. Masui, J.A. Gardella Jr., U. Singisetti, Ga_2O_3 MOSFETs Using spin-on-glass source/drain doping technology, *IEEE Electron. Device Lett.* 38 (2017) 513–516.
- [9] Z. Galazka, R. Uecker, D. Klimm, K. Irmscher, M. Naumann, M. Pietsch, A. Kwasniewski, R. Bertram, S. Ganschow, M. Bickermann, Scaling-up of Bulk $\beta\text{-}\text{Ga}_2\text{O}_3$ Single Crystals by the Czochralski Method, vol. 6, 2017, pp. Q3007–Q3011.
- [10] M. Baldini, M. Albrecht, A. Fiedler, K. Irmscher, R. Schewski, G. Wagner, Si- and Sn-doped Homoepitaxial $\beta\text{-}\text{Ga}_2\text{O}_3$ Layers Grown by MOVPE on (010) -oriented Substrates, vol. 6, 2017, pp. Q3040–Q3044.
- [11] M. Higashiwaki, K. Sasaki, H. Murakami, Y. Kumagai, A. Koukitu, A. Kuramata, T. Masui, S. Yamakoshi, Recent progress in Ga_2O_3 power devices, *Semicond. Sci. Technol.* 31 (2016), 034001.
- [12] A.J. Green, K.D. Chabak, E.R. Heller, R.C. Fitch, M. Baldini, A. Fiedler, K. Irmscher, G. Wagner, Z. Galazka, S.E. Tetlak, A. Crespo, K. Leedy, G.H. Jessen, 3.8-MV/cm breakdown strength of MOVPE-grown Sn-doped $\beta\text{-}\text{Ga}_2\text{O}_3$ MOSFETs, *IEEE Electron. Device Lett.* 37 (2016) 902–905.
- [13] M.H. Wong, K. Sasaki, A. Kuramata, S. Yamakoshi, M. Higashiwaki, Field-plated Ga_2O_3 MOSFETs with a breakdown voltage of over 750 V, *IEEE Electron. Device Lett.* 37 (2016) 212–215.
- [14] J. Kim, S. Oh, M.A. Mastro, J. Kim, Exfoliated $\beta\text{-}\text{Ga}_2\text{O}_3$ nano-belt field-effect transistors for air-stable high power and high temperature electronics, *Phys. Chem. Chem. Phys.* 18 (2016) 15760–15764.
- [15] S. Ahn, F. Ren, J. Kim, S. Oh, J. Kim, M.A. Mastro, S.J. Pearton, Effect of front and back gates on $\beta\text{-}\text{Ga}_2\text{O}_3$ nano-belt field-effect transistors, *Appl. Phys. Lett.* 109 (2016), 062102.
- [16] E.G. Villora, K. Shimamura, T. Ujiiie, K. Aoki, Electrical conductivity and lattice expansion of $\beta\text{-}\text{Ga}_2\text{O}_3$ below room temperature, *Appl. Phys. Lett.* 92 (2008), 202118.
- [17] Z. Galazka, K. Irmscher, R. Uecker, R. Bertram, M. Pietsch, A. Kwasniewski, M. Naumann, T. Schulz, R. Schewski, D. Klimm, M. Bickermann, On the bulk $\beta\text{-}\text{Ga}_2\text{O}_3$ single crystals grown by the Czochralski method, *J. Cryst. Growth* 404 (2014) 184–191.
- [18] Z. Guo, A. Verma, X. Wu, F. Sun, A. Hickman, T. Masui, A. Kuramata, M. Higashiwaki, D. Jena, T. Luo, Anisotropic thermal conductivity in single crystal β -gallium oxide, *Appl. Phys. Lett.* 106 (2015) 111909.
- [19] M. Slomski, N. Blumenschein, P.P. Paskov, J.F. Muth, T. Paskova, Anisotropic thermal conductivity of $\beta\text{-}\text{Ga}_2\text{O}_3$ at elevated temperatures: effect of Sn and Fe dopants, *J. Appl. Phys.* 121 (2017), 235104.
- [20] S. Ohira, N. Arai, Wet chemical etching behavior of $\beta\text{-}\text{Ga}_2\text{O}_3$ single crystal, *Phys. Status Solidi C* 5 (2008) 3116–3118.
- [21] T. Oshima, T. Okuno, N. Arai, Y. Kobayashi, S. Fujita, Wet etching of $\beta\text{-}\text{Ga}_2\text{O}_3$ substrates, *Jpn. J. Appl. Phys.* 48 (2009), 040208.
- [22] M. Passlack, E.F. Schubert, W.S. Hobson, M. Hong, N. Moriya, S.N.G. Chu, K. Konstadinidis, J.P. Manneaerts, M.L. Schnoes, G.J. Zydzik, Ga_2O_3 films for electronic and optoelectronic applications, *J. Appl. Phys.* 77 (1995) 686.
- [23] F. Ren, M. Hong, J.P. Manneaerts, J.R. Lothian, A.Y. Cho, Wet chemical and plasma etching of Ga_2O_3 (Gd_2O_3), *J. Electrochem. Soc.* 144 (1997) L239–L241.
- [24] J.E. Hogan, S.W. Kaun, E. Ahmadi, Y. Oshima, J.S. Speck, Chlorine-based dry etching of $\beta\text{-}\text{Ga}_2\text{O}_3$, *Semicond. Sci. Technol.* 31 (2016), 065006.
- [25] Y. Yao, R. Gangireddy, J. Kim, K.K. Das, R.F. Davis, L.M. Porter, Electrical behavior of $\beta\text{-}\text{Ga}_2\text{O}_3$ Schottky diodes with different Schottky metals, *J. Vac. Sci. Technol. B* 35 (2017), 03D113.
- [26] K.H. Baik, H.Y. Song, S.M. Hwang, Y. Jung, J. Ahn, J. Kim, Etched Surface Morphology of Heteroepitaxial Nonpolar (11-20) and Semipolar (11-22) GaN Films by Photoenhanced Chemical Wet Etching, vol. 158, 2011, pp. D196–D199.
- [27] Y. Jung, J. Ahn, K.H. Baik, D. Kim, S.J. Pearton, F. Ren, J. Kim, Chemical Etch Characteristics of N-face and Ga-face GaN by Phosphoric Acid and Potassium Hydroxide Solutions, vol. 159, 2012, pp. H117–H120.
- [28] L. Dong, R. Jia, B. Xin, B. Peng, Y. Zhang, Effects of oxygen vacancies on the structural and optical properties of $\beta\text{-}\text{Ga}_2\text{O}_3$, *Sci. Rep.* 7 (2017) 40160.
- [29] W. Mi, C. Luan, Z. Li, C. Zhao, X. Feng, J. Ma, Ultraviolet–green photoluminescence of $\beta\text{-}\text{Ga}_2\text{O}_3$ films deposited on $\text{MgAlO}_10(100)$ substrate, *Opt. Mater.* 35 (2013) 2624–2628.
- [30] L.L. Liu, M.K. Li, D.Q. Yu, J. Zhang, H. Zhang, C. Qian, Z. Yang, Fabrication and characteristics of N-doped $\beta\text{-}\text{Ga}_2\text{O}_3$ nanowires, *Appl. Phys. A* 98 (2010) 831–835.
- [31] L. Binet, D. Gourier, Origin of the blue luminescence of $\beta\text{-}\text{Ga}_2\text{O}_3$, *J. Phys. Chem. Solids* 59 (1998) 1241–1249.
- [32] K.W. Chang, J.J. Wu, Low-temperature Growth of Well-aligned $\beta\text{-}\text{Ga}_2\text{O}_3$ Nanowires from a Single-source Organometallic Precursor, vol. 16, 2004, pp. 545–549.
- [33] Z. Hajnal, J. Miró, G. Kiss, F. Réti, P. Deák, R.C. Herndon, J.M. Kuperberg, Role of oxygen vacancy defect states in the n-type conduction of $\beta\text{-}\text{Ga}_2\text{O}_3$, *J. Appl. Phys.* 86 (1999) 3792.
- [34] T. Zacherle, P.C. Schmidt, M. Martin, Ab initio calculations on the defect structure of $\beta\text{-}\text{Ga}_2\text{O}_3$, *Phys. Rev. B* 87 (2013), 235206.
- [35] J.B. Varley, J.R. Weber, A. Janotti, C.G. Van de Walle, Oxygen vacancies and donor impurities in $\beta\text{-}\text{Ga}_2\text{O}_3$, *Appl. Phys. Lett.* 97 (2010), 142106.
- [36] T. Harwig, F. Kellendonk, S. Slappendel, The ultraviolet luminescence of β -

- gallium sesquioxide, *J. Phys. Chem. Solids* 39 (1978) 675–680.
- [37] G. Blasse, A. Bril, Some observations on the luminescence of β - Ga_2O_3 , *Solid State Commun* 7 (1969) iii–iv.
- [38] T. Harwig, F. Kellendonk, Some observations on the photoluminescence of doped β -gallium sesquioxide, *J. Solid State Chem.* 24 (1978) 255–263.
- [39] J. Åhman, G. Svensson, J. Albertsson, A reinvestigation of β -gallium oxide, *Acta Crystallogr., Sect. C: Cryst. Struct. Commun.* 52 (1996) 1336–1338.
- [40] S. Geller, Crystal structure of β - Ga_2O_3 , *J. Chem. Phys.* 33 (1960) 676.
- [41] V.M. Bermudez, The structure of low-index surfaces of β - Ga_2O_3 , *Chem. Phys.* 323 (2006) 193–203.
- [42] S. Kumar, R. Singh, Nanofunctional gallium oxide (Ga_2O_3) nanowires/nanostructures and their applications in nanodevices, *Phys. Status Solidi RRL* 7 (2013) 781–792.
- [43] S.J. Pearton, J.C. Zolper, R.J. Shul, F. Ren, GaN: processing, defects, and devices, *J. Appl. Phys.* 86 (1999) 1–78.
- [44] W. Mönch, On the band-structure lineup at Ga_2O_3 , Gd_2O_3 , and Ga_2O_3 (Gd_2O_3) heterostructures and Ga_2O_3 Schottky contacts, *J. Mater. Sci. Mater. Electron.* 27 (2016) 1444–1448.
- [45] T.C. Lovejoy, R. Chen, X. Zheng, E.G. Villora, K. Shimamura, H. Yoshikawa, Y. Yamashita, S. Ueda, K. Kobayashi, S.T. Dunham, F.S. Ohuchi, M.A. Olmstead, Band bending and surface defects in β - Ga_2O_3 , *Appl. Phys. Lett.* 100 (2012) 181602.
- [46] A. Navarro-Quezada, Z. Galazka, S. Alamé, D. Skuridina, P. Vogt, N. Esser, Surface properties of annealed semiconducting β - Ga_2O_3 (100) single crystals for epitaxy, *Appl. Surf. Sci.* 349 (2015) 368–373.
- [47] D. Splith, S. Müller, F. Schmidt, H. von Wenckstern, J.J. van Rensburg, W.E. Meyer, M. Grundmann, Determination of the mean and the homogeneous barrier height of Cu Schottky contacts on heteroepitaxial β - Ga_2O_3 thin films grown by pulsed laser deposition, *Phys. Status Solidi A* 211 (2014) 40–47.
- [48] S. Müller, H. von Wenckstern, F. Schmidt, D. Splith, F.L. Schein, H. Frenzel, M. Grundmann, Comparison of Schottky Contacts on β -gallium Oxide Thin Films and Bulk Crystals, vol. 8, 2015, 121102.
- [49] S. Müller, H. von Wenckstern, F. Schmidt, D. Splith, H. Frenzel, M. Grundmann, Method of choice for the fabrication of high-quality β -gallium oxide-based Schottky diodes, *Semicond. Sci. Technol.* 32 (2017), 065013.